Conformational Dynamics of Dry Lamellar Crystals of Sugar Based Lipids: An Atomistic Simulation Study

Vijayan ManickamAchari[1,3], Richard A. Bryce[2], Rauzah Hashim[1,3]*

1 Department of Chemistry, University of Malaya, Kuala Lumpur, Malaysia, 2 Manchester Pharmacy School, University of Manchester, Manchester, United Kingdom, 3 Kavli Institute of Theoretical Physics China, Chinese Academy of Sciences, Beijing, China

Abstract

The rational design of a glycolipid application (e.g. drug delivery) with a tailored property depends on the detailed understanding of its structure and dynamics. Because of the complexity of sugar stereochemistry, we have undertaken a simulation study on the conformational dynamics of a set of synthetic glycosides with different sugar groups and chain design, namely dodecyl β-maltoside, dodecyl β-cellobioside, dodecyl β-isomaltoside and a $C_{12}C_{10}$ branched β-maltoside under anhydrous conditions. We examined the chain structure in detail, including the chain packing, *gauche/trans* conformations and chain tilting. In addition, we also investigated the rotational dynamics of the headgroup and alkyl chains. Monoalkylated glycosides possess a small amount of *gauche* conformers (~20%) in the hydrophobic region of the lamellar crystal (L_C) phase. In contrast, the branched chain glycolipid in the fluid L_α phase has a high *gauche* population of up to ~40%. Rotational diffusion analysis reveals that the carbons closest to the headgroup have the highest correlation times. Furthermore, its value depends on sugar type, where the rotational dynamics of an isomaltose was found to be 11–15% and more restrained near the sugar, possibly due to the chain disorder and partial inter-digitation compared to the other monoalkylated lipids. Intriguingly, the present simulation demonstrates the chain from the branched glycolipid bilayer has the ability to enter into the hydrophilic region. This interesting feature of the anhydrous glycolipid bilayer simulation appears to arise from a combination of lipid crowding and the amphoteric nature of the sugar headgroups.

Introduction

Glycolipid surfactant is cheap, non-ionic, and biodegradable [1] with a wide range of applications from emulsifiers, delivery systems to solubilization and extraction of membrane proteins [2]. Other features like low toxicity, low immunogenicity and specific sugar-cell recognition have broadened further the scope of interest in this material, including many fundamental studies. Glycolipids also exist naturally as a minor component in cell membranes, such as those found in Gram positive bacteria [3] and in the photosynthetic membranes of green plants [4]. But extracting them from natural products is challenging, and not cost effective. Therefore, highly pure synthetic glycolipids are usually used for applications and research studies. The amphiphilic nature of these lipids, both hydrophilic and hydrophobic, enable them to self-assemble into micelles, hexagonal phases, bilayers and other complex three dimensional cubic structures, generally in polar solvent, mainly water or even in dry conditions, as described recently [5–10]. Amongst these, the two-dimensional lipid bilayer is more important for its close resemblance to that of a phospholipid which is usually used to model the plasma- membrane [11]. Within a simple lipid bilayer structure, there exists detailed variation leading to a variety of mesophases, due to effects such as solvent type, concentration and temperature. For example, a hydrated bilayer is classified as a liquid crystalline (L_α) phase, in which the alkyl chains are disordered above the main transition temperature, T_C, while below that, the system assumes a gel phase (L_β), where the extended lipid chains tilt to the normal of the bilayer. At a much lower temperature, the bilayer forms a lamellar crystalline phase (L_C) where the extended lipid chains now have much lower tilting angles relative to those in the gel phase [12]. At zero or at a very low hydration, most of the lipids form a lamellar crystalline (L_C) phase [6,13,14]. Usually these lamellar phases show both long and short range order similar to a true crystal [14]. Meanwhile, other factors such as the molecular geometry, chain design and headgroup size influence the occurrence of these phases [12]. For example, monoalkylated glycolipids, at room temperature and under dry conditions, usually exist in the lamellar crystal phase (L_C) [15].

Bilayers of phospholipids have been studied extensively [16,17] compared to those of glycolipids, primarily due to the challenging task of dealing with the sugar's stereochemistry [5]. Thus, to unravel the glycolipid's complexity, a systematic structure property relationship study is useful. Investigation of these systems in the anhydrous state is also necessary to understand the detailed behavior of individual lipids uncomplicated by the presence of solvent. Recently some synthetic glycolipids bilayers have been studied in dry as well as hydrated forms [18,19], including dodecyl β-maltoside (βMal-C_{12}) which exists in an L_C phase over a temperature range of 20–80°C [19]. Within this range, this phase

has low thermal fluctuation and may give interesting properties different from phospholipids under anhydrous conditions [20]. However, glycolipids are highly hygroscopic; hence, it is difficult to have a completely pure and dry substance under normal experimental conditions.

Considering these points, we have undertaken a molecular dynamics simulation study using full atomistic resolution on four synthetic glycolipids namely, dodecyl β-maltoside (βMal-C$_{12}$, Figure 1a), dodecyl β-cellobioside (βCel-C$_{12}$, Figure 1b), dodecyl β-isomaltoside (βIsoMal-C$_{12}$, Figure 1c) in the L$_C$ phase and a branched chain maltoside (βBCMal-C$_{12}$C$_{10}$, Figure 1d) in the L$_\alpha$ phase. The liquid crystalline fluid phase (L$_\alpha$) is known to possess complex motions covering a wide range of time scales. Motions in the picosecond range include chemical bond vibration and torsional oscillation, while rotations, *gauche/trans* isomerization, and lipid wobbling occur over nanoseconds. Slow dynamics from milliseconds to hours are usually associated with the in-plane lateral diffusion, undulation and flip-flop of lipids [21]. In addition the amphoteric nature of sugar makes the dynamics of these carbohydrate liquid crystal phases even more intriguing and challenging. Therefore, we have extended our investigation into the conformational dynamical behavior of glycolipids in an anhydrous form to understand how these properties relate to the sugar stereochemistry and the lipid chain architecture.

Materials and Methods

Lipid Model Construction

Using IUPAC nomenclature, [23,24] the relative orientation of a reducing and a non-reducing sugar in disaccharides of βMal-C$_{12}$ and Cel-C$_{12}$ are represented by the dihedral angles (Φ and Ψ) of H1-C1-O1-C4' and C1-O1- C4'-H4' respectively. For an isomaltoside (βIsoMal-C$_{12}$), these are Φ (O5-C1-O1-C6'), Ψ (C1-O1-C6'-C5') and ω (O1-C6'-C5'-C4'). Initial values of Φ, Ψ and ω for these glycosides were obtained from the literature [23,25,26] (for details see Table S1). Using this information, the starting monomeric structures of these glycolipids were modeled and geometrically optimized using the HyperChem package [27]. A single monolayer with an 8×8 lipids was built and was geometry optimized. This monolayer was used to form a bilayer with the tail group of the lipids pointing towards each other and headgroups facing the opposite directions. Since there is no single crystal structure information available for βMal-C$_{12}$ [19], we have used crystal builder option in HyperChem to build the single bilayer. Then, the bilayer was replicated to form a second bilayer to give a simulation cell with a total of 256 lipids. The double bilayer system was used to resemble closely the experimental (lamellar) conditions [28]. A recent study by Abe *et al.* supports the assertion that the alkyl chains of glycolipid in L$_C$ phase are not perpendicular to the bilayer normal but tilted slightly [29]. Additionally, Abeygunaratne *et al.* also provide information on the tilt glycolipid structure in the smectic C liquid crystals by using optical microscopic and the electric polarization experimental methods [30]. Taking these observations into consideration, in our model, we have pre-tilted the lipid chains at about 15° to the bilayer normal. At the same temperature, the branched chain glycolipids give an anhydrous fluid L$_\alpha$ phase [31].

Simulation Details

MD simulations were performed using the AMBER molecular dynamics package [32] with force field parameter sets GLY-CAM_06d [33] and *ff99* [32] for the lipid head and tail respectively. An equilibration procedure was applied, involving restrained energy minimizations on tail and headgroup moieties

separately. The system was then heated gradually over 2 ns from 0 to 27°C in the *NVT* ensemble using the Andersen thermostat ($\tau_{TP} = 0.5$ ps) [34]. Upon reaching 27°C, the restraints were reduced on the lipids stepwise in the *NpT* ensemble using weak anisotropic pressure coupling, $\tau_P = 2$ ps. A time step of 1 fs was used with the SHAKE algorithm [35,36] to constrain covalent bonds involving hydrogen. Periodic boundary conditions were applied to the simulation box and long-range electrostatics for non-bonded interactions were treated using the particle mesh Ewald method [37,38]. We reprise our earlier 150–180 ns simulations of these systems [22], performing replicate simulations of 200 ns within the *NpT* ensemble at 27°C, but permitting fully anisotropic pressure scaling, as opposed to the isotropic conditions used previously. The trajectory coordinates were archived every 5 ps. As bilayers need at least 20 ns run to equilibrate [39], the last 160 ns of each 200 ns simulation was used for analysis. These simulations were performed with the GPU-accelerated version of the *pmemd* module.

Analysis

Area per head group and local density profile. Conventionally, the stability of the four bilayer assemblies, βMal-C$_{12}$, βCel-C$_{12}$, βIsoMal-C$_{12}$, and βBCMal-C$_{12}$C$_{10}$ were monitored over the entire simulation by observing properties such as the surface area per lipid at the interface (A) and the local density profile (LDP) [39,40]. The former (A) was estimated by applying a standard procedure, dividing the area of x–y plane by the number of lipids present in a leaflet (Figure S2) [41], while, the latter was obtained from the average of five 40 ns block averages of the 200 ns simulation (Figure S3). This block-averaged LDP profile is useful in evaluation of the convergence of the simulation with respect to the distribution of sugar and chain residues within the simulated system [39].

Radial distribution function

The packing of alkyl chains in the hydrophobic region was determined by calculating the radial distribution function (RDF) for selected carbon atoms on a lipid to the neighbouring lipids [42]. The RDF function $g(r)$ is obtained from

$$g(r) = N(r)/(4\pi r^2 \rho \delta r), \qquad (1)$$

where, $N(r)$ is the number of selected atoms between distance r and $r + \delta r$ from the reference atom. ρ is the number density [43]. We choose three carbon atoms, namely C72, C76 and C81, along a lipid chain from each monoalkylated glycosides corresponding to: near sugar moiety, middle and near to methyl group. The related RDFs were calculated using the *ptraj* module in AMBER.

Gauche and trans population distribution. Alkyl chains may contain several methylene groups, whose conformations [44] determine the detailed phase behavior [45]. These conformations were analysed by calculating the probability, $P(\theta)$ of the *gauche/trans* conformers, defined as,

$$P(\theta) = \left\{ \begin{array}{l} 1(\theta \geq (2/3)\pi, \text{ trans state}) \\ -1(\theta < (2/3)\pi, \text{ gauche state}) \end{array} \right\}, \qquad (2)$$

where θ is the dihedral angle formed by four consecutive carbons along the alkyl chain [17]. The *ptraj* module in AMBER was used to evaluate this probability function.

Autocorrelation function. To understand the dynamics of glycolipids in the self-assembled system, rotational motions of the alkyl chain and sugar headgroup have been examined separately.
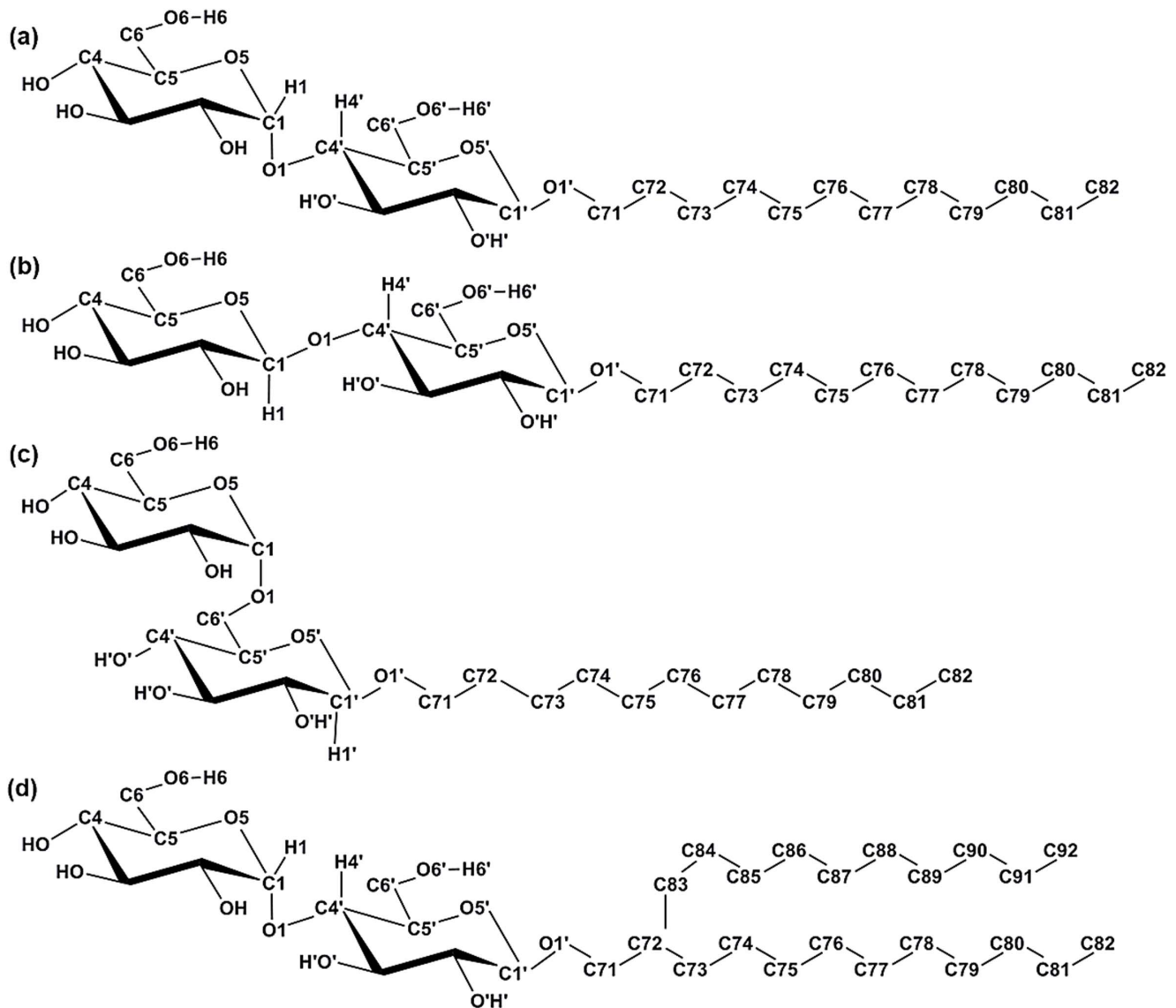
Figure 1. Glycosides used in the simulation: (a) βMal-C$_{12}$ (b) βCel-C$_{12}$ and (c) βIsoMal-C$_{12}$ (d) βBCMal-C$_{12}$C$_{10}$. Starting from glycosidic oxygen, each glycolipid's main alkyl chain (sn-1) is labeled from C71 to C82 and the branched chain (sn-2) from C83 to C92. Here, for clarity we have reduced the atoms' labels on the sugar, a slight modification from the standard nomenclature according to IUPAC given in Figure 1 of [22].
doi:10.1371/journal.pone.0101110.g001

For the headgroup, we selected three rotational systems namely, the reducing sugar (ring2), non-reducing sugar (ring1) and the combined sugar rings (ring12), represented by the appropriate unit vectors, $\vec{\mu}_{ring2}$ from C1 to C4, $\vec{\mu}_{ring1}$ from C1' to C4', and $\vec{\mu}_{ring12}$ from C1' to C4 respectively (see Figure S1(a)). For the rotational diffusion of the chain region, the C–H vectors along the alkyl chain were chosen. Using these vectors and *ptraj* module from AMBER the correlation times for the various motions were estimated using the second rank reorientational autocorrelation functions, $C_2(t)$ defined by [46]:

$$C_2(t) = \frac{1}{2}\langle 3[\vec{\mu}(t)\cdot\vec{\mu}(0)]^2 - 1\rangle, \qquad (3)$$

where $\vec{\mu}(t)$ is a unit vector of the chosen rotational mode. $C_2(t)$ was evaluated for each lipid over the production trajectory and averaged over the number of lipids within the system. The average

$C_2(t)$ was fitted to a single-exponential function; from which the correlation time was obtained by integration using the trapezoidal rule. The standard deviation of $C_2(t)$ was also determined to within the range of ± 0.5 ns.

Results

Stability and structural properties of bilayers

In order to evaluate the equilibration of the four glycolipid bilayer systems, the time evolution of the surface area per lipid at the interface (A) and the local density profiles (LDP) were assessed over the 200 ns simulation (Figures S2 and S3 respectively). The four bilayer assemblies, βMal-C$_{12}$, βCel-C$_{12}$, βIsoMal-C$_{12}$, and βBCMal-C$_{12}$C$_{10}$, remained intact over the simulations and achieved equilibrium with respect to A and LDP by 40 ns. In the subsequent analyses, we therefore take the last 160 ns of each trajectory. The average area per lipid (A) and the d-spacing from

the LDPs during the production stage are given in Table 1. Compared to the reported values in [22], in our replicate simulations here, A for the four glycolipid systems are similar to within the error; the d-spacing differ by only about 3–16%. These variations could be attributed in part to the slight difference in simulation methodology: as opposed to the isotropic pressure scaling used in our previous study, here we apply fully anisotropic pressure scaling throughout the simulation, following the work of Doxastakis et al. [20] on simulating the melting of phospholipid membranes under anhydrous conditions.

Alkyl chain packing

The packing within the chain region for the βMal-C_{12}, βCel-C_{12} and βIsoMal-C_{12} was assessed by computing the radial distribution function, giving the particle density variation as a function of distance from a reference particle, selected to be the carbon atoms C72, C76, and C81 along the hydrophobic chain. For all the three monoalkylated systems, the principal peaks in the RDF are around 5.1, with the errors for βMal-C_{12} and βCel-C_{12} within ± 0.2 Å while for βIsoMal-C_{12} ± 0.5 Å, (Figure 2). The errors were estimated using 20 ns block averages. The RDF of βIsoMal-C_{12} shows a broader first maximum peak for all the three carbons along the alkyl chain (Figure 2c) compared to βMal-C_{12} and βCel-C_{12} (Figure 2a,b). While the peak locations are nearly the same for all systems, the broadening around the peak in the isomaltoside RDF is considerably larger than for the others, suggesting that the βIsoMal-C_{12} chains are less ordered compared to the other two monoalkylated lipids, despite being in the same phase. Furthermore, for isomaltoside, the second last carbon, C81, is more structured, while in the maltoside and cellobioside, it is the carbon closest to the headgroup, C72, which is more structured. To examine this observation visually, we have superimposed a vector (in yellow) for every chain in a given configuration snapshot (Figure 3). This figure points to a tighter packing in βCel-C_{12} compared to βMal-C_{12}, while for βIsoMal-C_{12} the chain vectors are more randomly orientated, due to an increase in lateral area related to the $\alpha(1–6)$ glycosidic linkage. It also appears that some of the sn-2 chain vectors of the branched chain maltoside appear to protrude into the sugar region (Figure 3), while such protrusions are less obvious for its sn-1 vectors. The protrusion of the branched chain maltoside will be discussed in detailed later.

Gauche-trans population for alkyl chain

The gauche populations were computed for the lipid chains for βMal-C_{12}, βCel-C_{12} and βIsoMal-C_{12} in their L_C phase (Figure 4a-c) and for βBCMal-$C_{12}C_{10}$ in the L_α phase (Figure 4d-e). We find the monoalkylated glycolipids possess a low proportion of gauche conformations relative to trans conformations; for example, the average gauche populations for βCel-C_{12} and for βMal-C_{12} are $14\pm3\%$ and $16\pm3\%$, respectively (Figure 4a,b). To within error, these results show that both βCel-C_{12} and βMal-C_{12} have similar gauche populations despite the fact that the former has two glucose units equatorially connected at the C1–O1 bond, while in the latter, the two units are axially connected (see Figure 1). The closely packed headgroups possibly induce the chains to align closer to each other, restricting isomeric rotation, and leading to fewer kinks or bending along the chain. βIsoMal-C_{12} has a higher predicted gauche population ($20\pm4\%$); its larger volume and area per lipid [22], correlates with more freely rotating and flexible chains. For the branched glycolipid, βBCMal-$C_{12}C_{10}$ (in the L_α phase), although it has the same headgroup as βMal-C_{12} (in the L_C phase), the branching at C72 (Figure 1d) gives an overall increase in volume and headgroup area A. This corresponds to a significant increase in gauche population in the branched chain sn-1 (Figure 4d). Additionally, the sn-2 chain possesses a gauche population ranging from 40% (close to the sugar head) to 10% (at the tail end). The gauche profiles for sn-1 and sn-2 (Figure 1d and e) look similar in general. However, upon closer examination within each leaflet, close to the headgroup, the first four gauche fractions differ slightly with no definite pattern. This slight differentiation may cause unequal flexibility or mean curvature between leaflets leading to bilayer asymmetry [48,49].

Rotational motion

Dynamics in the L_C phase is understandably limited compared to the L_α phase. Within this more restricted dynamical landscape, we seek to examine if there are dynamical features that differ as a function of stereochemical changes of glycolipid in the self-assembled system. To this end, we examine the rotational modes of the alkyl chain and sugar headgroups.

Alkyl chain

Generally, rotational diffusion in the anhydrous glycolipid systems is slow (on the nanosecond timescale) for the alkyl chain C–H vectors in the chain region, unlike those reported for

Table 1. Average values at 27°C of the simulated area per lipid, A and the bilayer spacing, d.

Lipids	Area per lipid, $A/\text{Å}^2$	Bilayer spacing, $d/\text{Å}$	Peak value of Chain tilt angle, $\theta°$
βMal-C_{12}	39.4±0.2 (38.8±0.2)	32.2±0.1 (32.9±0.5)	18±1 (18)
Experiment [19]	43 (20°C)	33.5 (20°C)	
		41.5 Å (at 80°C)	
βCel-C_{12}	39.2±0.2 (38.7±0.1)	34.1±0.1 (32.3±0.2)	15±1 (13)
βIsoMal-C_{12}	49.1±0.3 (48.6±0.2)	22.9±0.2 (26.6±0.6)	42, 59±3 (26)
βBCMal-$C_{12}C_{10}$	50.1±0.3 (51.9±0.2)	41.9±0.2 (36.1±0.2)	24, 156±3 (sn-1) (27)
βBCMal-$C_{12}C_{10}$			24, 156±3 (sn-2) (30)
Experiment [47]			
βMal-$C_{12}C_8$	53 (25°C)	36.2 (25°C)	
βMal-$C_{14}C_{10}$	58 (25°C)	36.9 (25°C)	

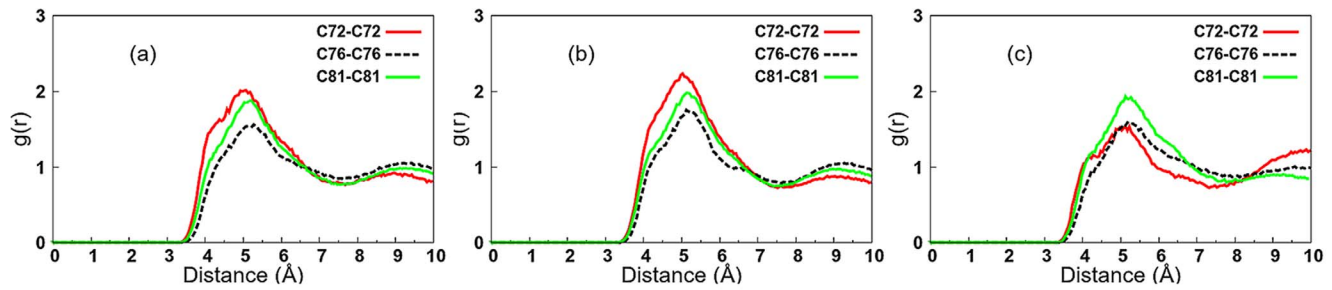(Values in parenthesis are from [22]).
doi:10.1371/journal.pone.0101110.t001

Figure 2. Radial distribution function for three carbon atoms along the alkyl chain for monoalkylated lipids: (a) βMal-C_{12} (b) βCel-C_{12} and (c) βIsoMal-C_{12}.
doi:10.1371/journal.pone.0101110.g002

hydrated phospholipid bilayers in an L_{α} phase [46,50]. The general appearance of the rotational autocorrelation functions $C_2(t)$ is similar for all the systems (Figure S5). However, upon closer scrutiny (Figure 5), the correlation times of the C–H vectors next to the sugar group are higher than those vectors further away from the sugar group. This observation agrees with a recent study on an anhydrous DPPC (dipalmitoylphosphatidylcholine) bilayer [20] suggesting the tail region closer to the headgroup is mainly experiencing vibrations, with only a small number of conformation transitions.

When compared to the chains of βCel-C_{12} and βMal-C_{12}, the alkyl chain of βIsoMal-C_{12} shows slightly higher $C_2(t)$ values for carbons close to the headgroup (Figure 5). For example, C71 has a correlation time about 45 ns compared to 40 and 38 ns for βCel-C_{12} and βMal-C_{12} respectively (Figure 5). However, towards the end of the tail, the alkyl chain of βIsoMal-C_{12} has slightly lower correlation times compared to βCel-C_{12} and βMal-C_{12}.Thus, the alkyl chain carbons of βIsoMal-C_{12} appear to be more restricted in rotational motion involving carbons near the headgroup compared to the tail; the latter effect correlates with the chain disorder and partial interdigitation of βIsoMal-C_{12} compared to the other monoalkylated lipids (Figure 3). In the βBCMal-$C_{12}C_{10}$ system, the first two carbons in *sn-1* chains show higher correlation time compared to those in the monoalkylated systems. On the other hand the rest of the carbons behave similarly, as those in the single chain lipids, including *sn-2*.

Sugar head

A disaccharide unit contains two simple sugars connected via a flexible glycosidic bond, which allows each sugar moiety to rotate

within its vicinity. We have determined the rotational diffusion of the sugars at the headgroup region using equation 3. Figure S6 shows the autocorrelation profiles for the non-reducing sugar (*ring1*), reducing sugar (*ring2*) and both sugars together (*ring12*), while Figure 6 gives the corresponding correlation times.

In general the non-reducing sugar (*ring2*) has slightly faster rotational diffusion than the reducing sugar (*ring1*) and the combined sugar headgroup (*ring12*). In particular for βIsoMal-C_{12}, the non-reducing sugar's correlation time (τ_{ring2}) on average is the smallest, which is consistent with the fact that this lipid has a smaller *d*-spacing and a larger *A* compared to the other glycolipid systems. Depending on the stereochemistry, the headgroup correlation time of the lipid headgroup differs only slightly such that, τ_{ring12} of βMal-C_{12} (with a α(1–4)-linkage) and βCel-C_{12} (with an β(1–4)-linkage) is 78 and 80 ns respectively. The τ_{ring12} values for βMal-C_{12} and βIsoMal-C_{12} are also similar, despite the structural difference in the headgroup. The similarity in this dynamical behavior can be related to the distributions of hydrogen bonds in both βMal-C_{12} and βIsoMal-C_{12}. In both disaccharides, the major hydrogen bonding occurs at the hydroxymethyl group on the non-reducing sugar, such that the O6 acts as an acceptor while the HO6 acts as a donor. However, the next most dominant hydrogen bond site is O6' in βMal-C_{12}, but O1' in βIsoMal-C_{12} (see Figure 7: (a) and (d) from [22]). In βMal-C_{12} the O6'-HO6' group (see Figure 1) acts as donor and acceptor, while in βIsoMal-C_{12} the O1' acts only as an acceptor. It was also found that the headgroup correlation time, τ_{ring12}, for the branched glycolipid is shorter (hence faster rotational diffusion) compared to the monoalkylated one, even though both βMal-C_{12} and βBCMal-$C_{12}C_{10}$ have the same sugar group. We note that the branched
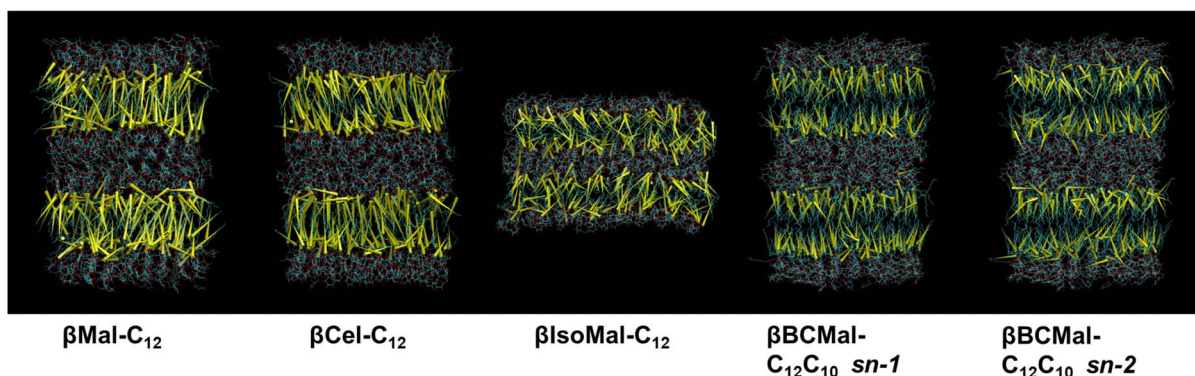

Figure 3. Snapshot of chain vectors between midpoints of C71–C72 and C80–C81 for monoalkylated lipids and chain *sn-1*. For chain *sn-2*, the vector is defined between midpoints of C71–C72 and C90–C91.
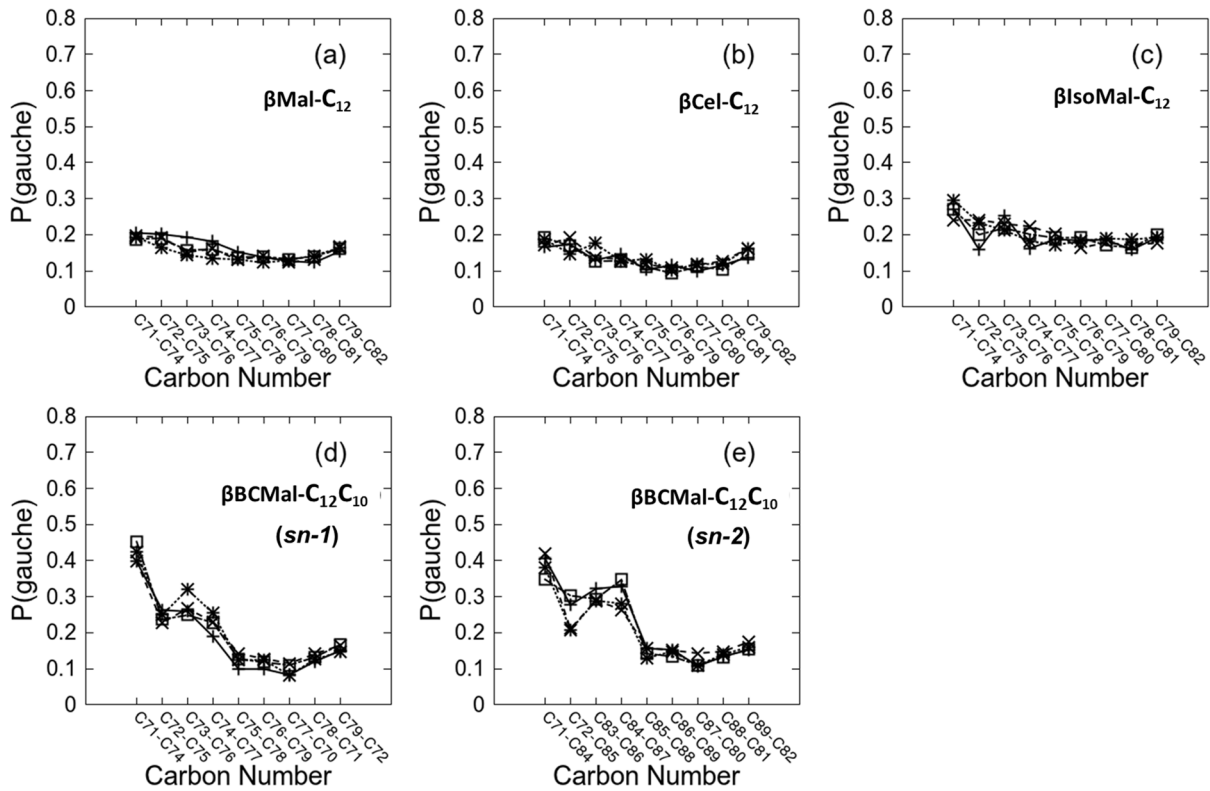doi:10.1371/journal.pone.0101110.g003

Figure 4. Fractional *gauche* population in, *P*(*gauche*), for dihedral angles between carbons in the alkyl chains. The dihedral angle label, for example C71–C74 represent C71–C72–C73–C4 following alkyl chain numbering in Figure 1. (a) *β*Mal-C$_{12}$, (b) *β*Cel-C$_{12}$, (c) *β*IsoMal-C$_{12}$, (d) *β*BCMal-C$_{12}$C$_{10}$(*sn-1*), and (e) *β*BCMal-C$_{12}$C$_{10}$(*sn-2*). First lipid layer (□), second layer (×), third layer (+), and fourth layer (*).
doi:10.1371/journal.pone.0101110.g004

glycolipid exists in the L$_\alpha$ phase, where the constituent lipid chains tend to be more flexible, with many modes of motions, and the headgroup moiety is subjected to a greater motion due to the increased area per headgroup.

Chain tilting

The chain tilting behavior was analysed by choosing a vector from the midpoints of C71–C72 and C81–C82 for the mono-alkylated and the *sn-1* chains, while for the *sn-2* chain, it is defined from the midpoints of C83–C84 and C91–C92 (see Figure S1(b)).

We plotted the distributions of these tilt angles using the first leaflet for the four systems (Figure 7). The maximum tilt values for *β*Cel-C$_{12}$ and *β*Mal-C$_{12}$ do not differ from the previous simulations [22], with values of 18° and 15° respectively (Table 1). Interestingly, for both the *β*IsoMal-C$_{12}$ and *β*BCMal-C$_{12}$C$_{10}$, the maximum tilt values differ and the profiles display a more prominent bimodal distribution. In the case of isomaltoside, the two maxima are at 43° and 59° (Figure 7), which accounts for the significantly smaller *d*-spacing compared to the other two glycolipid systems considered here. A tilt angle θ of zero implies
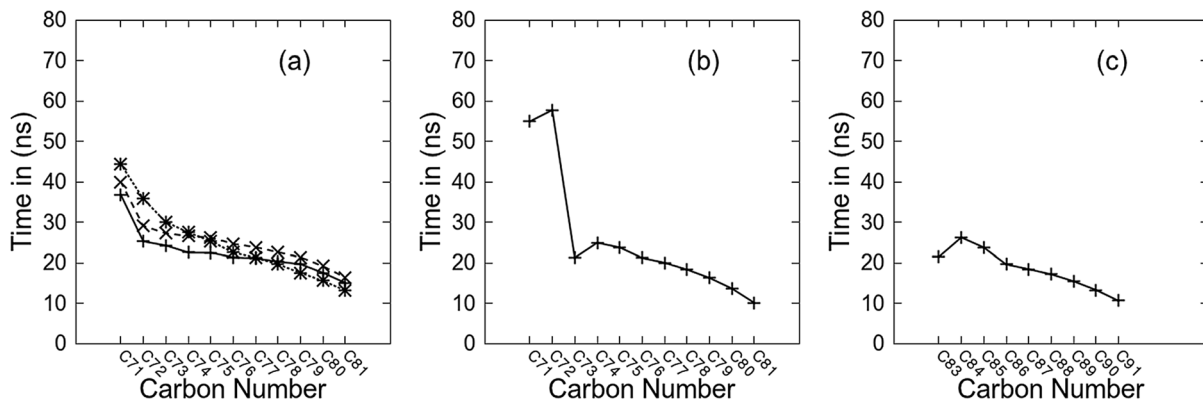

Figure 5. Correlation times as a function of each C–H vector along lipid alkyl chains are shown. The labeling of carbon atoms follows the naming convention as in Figure 1. (a) shows the correlation times for monoalkylated glycolipids, *β*Mal-C$_{12}$ (+), *β*Cel-C$_{12}$ (×), and *β*IsoMal-C$_{12}$ (*). (b) and (c) show correlation times for chains *sn-1* and *sn-2* respectively for *β*BCMal-C$_{12}$C$_{10}$.
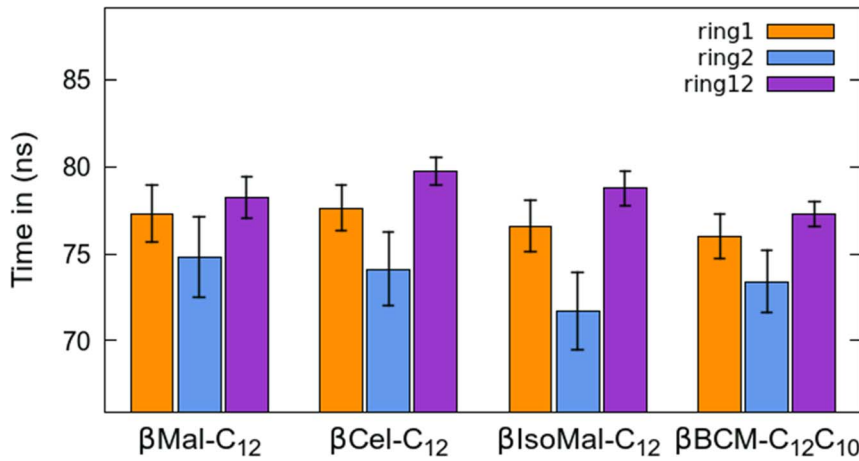doi:10.1371/journal.pone.0101110.g005

Figure 6. Average correlation time of sugar headgroup of lipids: reducing sugar (*ring1*); non-reducing sugar *(ring2)*; and combination of *ring1* and *ring2* (*ring12*).
doi:10.1371/journal.pone.0101110.g006

a perfect alignment of the chain vector with the layer normal, while a value of $180°$ implies the chain vector has "flipped" over. In the case of βIsoMal-C_{12}, the two peak values represent the most probable chain vector orientations possibly arising from the $\alpha(1–6)$ glycosidic linkage connecting the two glucose units. In the previous simulation [22], these peaks were small, but are more populated in the current study; whilst this may arise simply from the additional sampling of this replicate, it may also be due to the greater

freedom available to the system in using a fully anisotropic pressure scaling regime.

The branched chain glycoside is also bimodal in both the chain profiles. Firstly, the *sn-1* and *sn-2* chains have a non-zero population at the θ value of $90°$, meaning some chains are parallel to the bilayer. In addition, there are double peaks symmetrical about the $90°$ angle for both the two branched chains, indicating there are two possible conformations equally populated
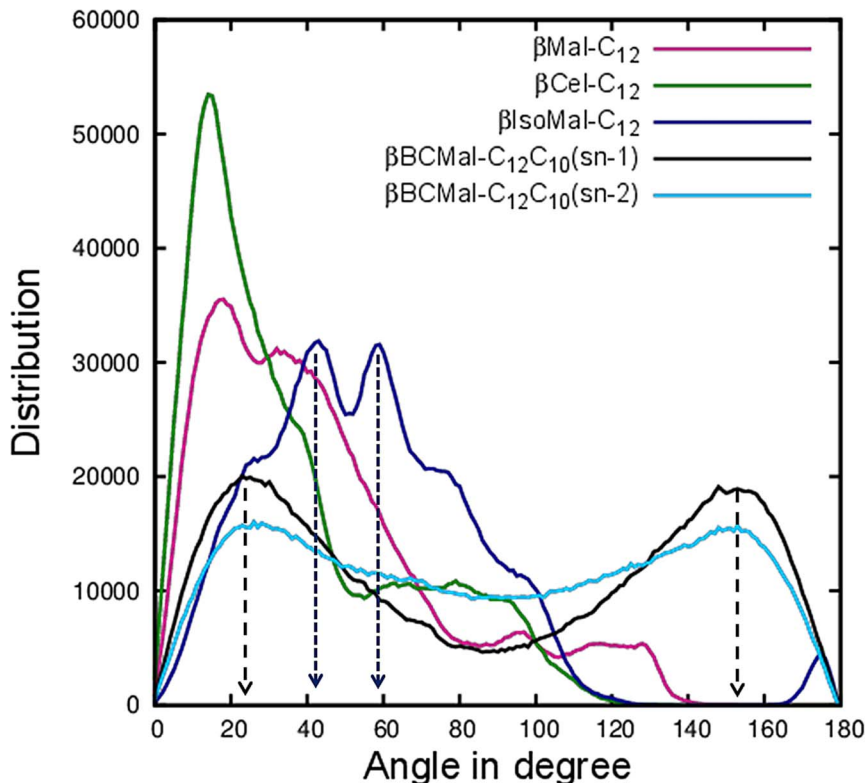
Figure 7. Distributions of alkyl chain tilt angle θ of various glycolipids for one layer. Shows the current results for 160 ns production runs for various glycoside systems in different colored lines, where medium violet red for βMal-C_{12}, black for βBCMal-$C_{12}C_{10}$ (*sn-1*), deep sky blue for βBCMal-$C_{12}C_{10}$(*sn-2*), green for βCel-C_{12} and dark blue for βIsoMal-C_{12}.
doi:10.1371/journal.pone.0101110.g007

at θ of 24° and 156°. To investigate this behavior and if it involves lipid flipping, we examined the glycolipid dynamics visually and found evidence of chain penetration into the hydrophilic headgroup region. As an example of this behavior, we present a movie of the last 160 ns production simulation, highlighting a lipid in the third leaflet (see Video S1 generated using VMD [51]). It is apparent over the course of the simulation that its chain works its way into the sugar headgroup environment. Based on the tilt angle distribution in Figure 7, we estimate for every leaflet there are about 10% of such lipids, which can be verified by examining the chain layer. We also present a movie focusing on the dynamics of the lipid headgroup region (Video S2); here we can see the emergence of the complementary hydrophobic cavity within the sugar region, which accommodates the lipid tail. From these dynamics visualization studies, we also discount the possibility of lipid flip. Nevertheless, by observing the movie and the way the chain vectors *sn-1* and *sn-2* are defined, these two peak conformations (θ of 24° and 156°) are possible as shown in Figure 8a, a snapshot captured from the movie. These results imply the chains can readily protrude into the hydrophilic region due to the formation of a "cavity" or "hole" in the headgroup region by sugar cooperative motion (Figure 8c), which is large enough to accommodate the alkyl chain. Figure 8d shows the time evolution of a selected lipid, whose alkyl chain made an attempt to associate itself with the headgroup region (represented by the wire and VDW model).

Discussion

We report 160 ns simulations of four glycosides namely βMal-C_{12}, βCel-C_{12}, βIsoMal-C_{12} and βBCMal-$C_{12}C_{10}$ in anhydrous bilayer assemblies, to understand the relationship of structural and dynamical properties to the stereochemistry of these sugar based lipids. The stereochemistry of the sugar group is known to affect profoundly the assembly states and our work here has provided further evidence especially in the chain and headgroup orderings,

structure and dynamics. For the three glycosides in the same L_C phase, the chains for βIsoMal-C_{12} are in a more disordered state compared to βCel-C_{12} and βMal-C_{12} (Figures 2 and 3). This is exemplified by the higher population of *gauche* chain dihedral conformations for βIsoMal-C_{12} compared to βCel-C_{12} and βMal-C_{12} (Figure 4). The lower ordering of the βIsoMal-C_{12} chains is most probably due to the increase in lateral area per lipid at the interface, which is related to the α(1–6) glycosidic linkage between two sugar moieties.

For the branched glycolipid, βBCMal-$C_{12}C_{10}$, which is in the L_α phase, a higher *gauche* population than for the monoalkylated lipid is observed although the systems are at the same temperature. Overall, this suggests the *gauche* population is influenced by chain branching and glycosidic linkage between two sugars, but less affected by the anomeric conformation or temperature. Consequently, the *gauche* populations affect some bilayer properties, including the bilayer *d*-spacing, as have been demonstrated experimentally from the study of anhydrous octyl β-maltoside (βMal-C_8) and decyl β-maltoside (βMal-C_{10}) bilayers using differential scanning calorimetry (DSC) and small angle x-ray scattering (SAXS) at ~25°C in the L_C phase. In this study, the measured bilayer *d*-spacing was different before and after the glass transition T_g [52]. The *gauche* population in the L_α phase is higher compared to the glass phase by 3% and 7% for βMal-C_8 and βMal-C_{10} respectively [52]. On cooling from the L_α phase into the glassy phase, both the systems retained their liquid crystalline chain ordering, because a longer time was needed for the chains to regain the all-*trans* conformation [52]. In addition, long chain alkyl maltosides, such as tetradecyl β-maltoside (βMal-C_{14}) and hexadecyl β-maltoside (βMal-C_{16}) in the anhydrous state have been studied [18]; both systems have the same melting temperature of about 105°C, but phases below this temperature are complex and strongly driven by kinetics, causing them to be metastable. The lamellar structure in the anhydrous low temperature crystal has a *d*-spacing of about 37 Å but in the anhydrous
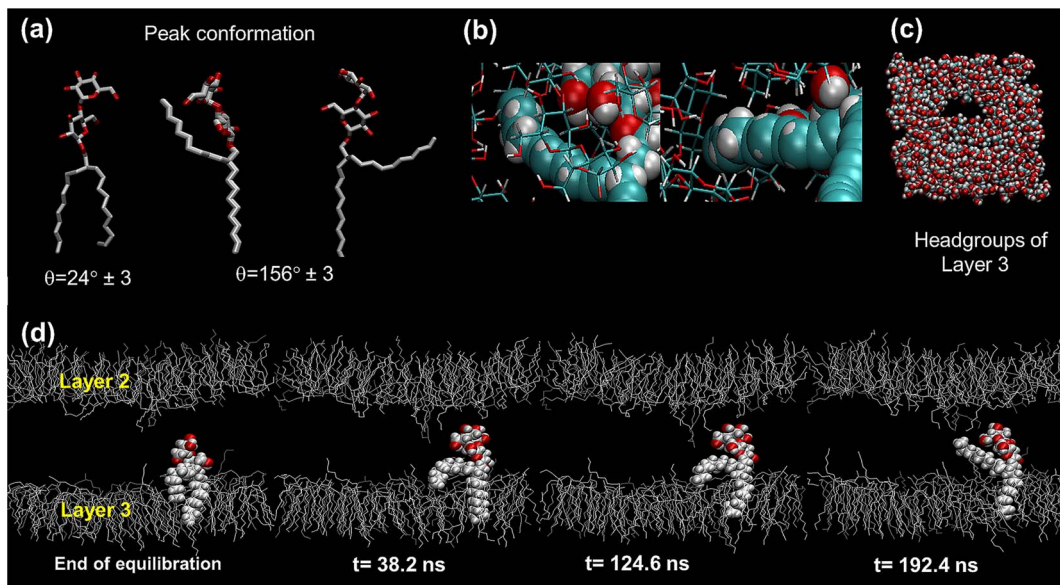

Figure 8. Some lipids' conformations and bilayer snapshots from the simulation. (a) Three possible lipid conformations with the chain tilt angle, θ of 24° and 156°. (b) The dispersion interaction observed from two viewing angles, between the C–H from the sugar face and those of the alkyl chain by a representative lipid (enlarged) from the third layer. (c) A characteristic example of the sugar headgroup region (t = 140 ns) from the third leaflet showing the hydrophobic cavity (top-view). (d) The time evolution of a typical side-view of the second and third leaflets. The lipid (drawn fully with VDW model) is seen to work itself into the hydrophilic region.
doi:10.1371/journal.pone.0101110.g008

high temperature crystal, the inter-lamellar distance is 43 Å. The difference of 6 Å (or 14%) could be attributed to the chain tilting together with the presence of an all-*trans* conformation in the anhydrous low temperature crystal (Figure S4). Meanwhile, the liquid crystalline state has a *d*-spacing about 40–41 Å (summary given in Table S2), where the value is closer to the *d*-spacing in the glass phase (Figure S4). But the ordered lamellar phase, which has the all-*trans* conformation for the chains, has about 7% less than the *d*-spacing (38 Å) compared to the L_α phase, which may be attributed to the tilted chain with respect to the bilayer normal. The presence of *gauche* conformations in the L_α phase reduces interdigitation, leading to a higher *d*-spacing relative to the other bilayer phases, except for the anhydrous high temperature crystal phase.

The sampling of chain conformations for the monoalkyl glycolipids in the lamellar crystalline phase, L_C, is further reflected by analysis of rotational diffusion (Figure 5). These lipid chains may interact non-specifically [53], where the carbon atoms in the chains are able to rotate in a limited fashion within the lattice, leading to partial local rotations along the chain, as observed previously in the L_β or the gel phases for example [54]. Although βMal-C_{12} and βBCMal-$C_{12}C_{10}$ have the same sugar headgroup, the carbons along the chain from both systems show different rotational behavior (Figure 5). This arises from the steric constraints of the two branching chains in βBCMal-$C_{12}C_{10}$; the resulting 'chain-overcrowding' in the hydrophobic region leads to the dominance of a repulsive van der Waals interaction. From our analysis of the autocorrelation function and visual inspection (Video S2), we note that the sugar headgroups also experience some partial "rotational motion", although much slower than the chain carbon partial rotation. Before leaving the subject on dynamics, we comment on one of the βIsoMal-C_{12} stereoisomers, namely the gentibioside, whose non-reducing sugar is attached to the reducing sugar by a $\beta(\tilde{1}6)$ linkage. The bilayer L_α phase of this gentibioside was studied using a ^{2}H-NMR by Carrier *et al.* [55], who found its headgroup dynamics is relatively slower compared to other glycolipids studied at that time. Qualitatively this finding perhaps could lend support for the observed difference in the dynamics of the isomaltose headgroup as compared to the other sugar lipids.

For phospholipid systems, there are extensive studies of headgroup dynamics focused specifically on the hydrophilic moiety's rotational diffusion, albeit mainly in aqueous solution [50,56,57]. Many phospholipid headgroups act only as hydrogen bonding acceptors [58] but the sugar groups in glycolipids are both acceptors and donors of hydrogen bonding. This property of the headgroup grants glycolipids a strong coupling with its neighboring lipid headgroups in the self-assembly. Moreover, the covalent framework of the sugar, containing aligned C–H groups as well as polar groups, leads to its amphoteric nature [59–61]. This important property of sugars increases the intra-layer hydrogen-bond interaction, self-assembly stability and makes the phase boundary temperature independent [62]. So the headgroup motion is highly restricted by the extensive hydrogen bonds with the neighboring lipids. A comparison of the studies of phospholipid and glycolipid surfactants under thermotropic conditions, by Huang and Li [63] and Auvray *et al.* [19] respectively, further illustrates the distinctive behavior of sugar lipids. In these studies, phosphatidylcholine lipids were reported to undergo a gel to liquid-crystalline transition at about 70°C, while, at nearly the same temperature, glycolipids such as βMal-C_{12} experienced a solid̃ solid phase transition, followed by a gel to liquid-crystalline phase transition at $\sim$103°C. Ericsson *et al.* [18] has suggested that the melting of alkyl-maltosides (from lamellar crystal to a liquid

crystal phase) is primarily governed by the nature of the headgroup rather than by the alkyl chain length, primarily due to the extensive inter-molecular hydrogen bonding within the headgroup.

Conventionally, the association of sugar headgroups with lipophilic alkyl tails is considered to be highly unfavourable. However, the amphoteric nature of the sugar headgroups here has made this possible: the lipid chain can associate itself with the hydrophobic face of the saccharide unit [64] (see Figure 8b). There are many examples of saccharide binding to aromatic groups, e.g. with the Tyr, Phe and Trp amino acid residues of proteins [65,66]. Our observation of chain-sugar association is not unreasonable, since other studies have appeared in recent years (e.g. [67]). The formation of hydrophobic cavities may provide the seeding condition for lipid flip-flop, a rare event, which may possibly be observed in a much longer simulation, even in an anhydrous bilayer system. A MD simulation which demonstrated lipid flip, performed by Gurtovenko and Vattulainen [68], suggested that the formation of a water hole in the hydrophobic region is an enabling condition for the flip motion. Our results point to the effects of chain crowding in forcing some lipids to protrude into the hydrophilic region. It is interesting to consider the possibility that, as these lipid tails vacate the hydrophobic cavity, the defects can permit seepage of water (if present) into these regions, potentially forming a pore for water. Therefore, our anhydrous branched chain glycolipid system, uncomplicated by the presence of solvent, may give insights into the formation of water defects in glycolipids [69].

Conclusion

Glycolipids, although present in a smaller quantity than phospholipids, are ubiquitous in cell membranes and exhibit a diverse range of structures. This suggests they are important in cell functions, for example, in cell aggregation and dissociation. A glycolipid is classified as an amphitropic liquid crystal, able to self-assemble in a dry or solvated environment through separation of the extensively hydrogen bonded hydrophilic region from that of the repulsive hydrophobic alkyl chain. Systematic examination of the structure and dynamics as a function of sugar stereochemistry and hydrocarbon chain is necessary to understand the complex organization within this self-assembly system. Complementing our earlier structural studies of these systems, we report a dynamical analysis of the three monoalkylated glycosides with maltose, cellobiose and isomaltose sugar headgroups in the lamellar crystal (L_C) phase and a branched chain maltoside in the lamellar (L_α) phase. Our simulations suggest that chain packing is not influenced significantly by the anomeric configuration at the glycosidic linkage that connects two headgroups. Thus, the $\beta(1–4)$ linked βCel-C_{12} has a similar packing to the $\alpha(1–4)$ linked βMal-C_{12}. On the other hand, the RDF of the $\alpha(1–6)$ link of βIsoMal-C_{12}, is in a marked contrast to these two, implying it has a more loosely packed structure. In the current study, where the lipids are at the room temperature, the chains do sample a small amount of *gauche* conformation. This suggests the L_C phase of these glycolipids is not entirely in a solid phase but possesses some chain disorder. We also observed the rotational dynamics of the headgroup and tail exhibit different behavior, where the headgroup rotates slower than the tail by a factor of at least two. Our simulations also suggest an unusual feature for the anhydrous bilayer system of branched chain glycolipids; in this system with its overcrowded chain region, the alkyl chains work themselves into the headgroup region and appear to associate with the more hydrophobic face of the sugar. Further work is necessary to

explore the generality of these alkyl chain saccharide headgroup interactions for a range of glycolipid systems. Nevertheless, together with the emerging concepts of lateral segregation, lipid flip and domain formation, these findings provide new insights into our understanding of membrane stability and integrity.

Supporting Information

Figure S1 Definition of vector $\vec{\mu}_{ring2}$ from C1 to C4, vector $\vec{\mu}_{ring1}$ C1' to C4' and $\vec{\mu}_{ring12}$ from C1' to C4 for the sugar groups. The chain vector $\vec{\mu}_{chain}$ (for all monoalkylated lipids) and $\vec{\mu}_{sn-1}$ (for sn-1 chain) are defined from the mid points between C71–C72 and C81–C82. For sn-2 chain, the vector $\vec{\mu}_{sn-2}$ is defined from the mid points between C83–C84 and C91–C92. (TIF)

Figure S2   Area per lipid of βMal-C$_{12}$, βCel-C$_{12}$, βIsoMal-C$_{12}$, and βBCMal-C$_{12}$C$_{10}$. (TIF)

Figure S3   Local density profile. Each plot comprises 40 ns blocks of averages.(a) βMal-C$_{12}$, (b) βCel-C$_{12}$, (c) βIsoMal-C$_{12}$, (d) βBCMal-C$_{12}$C$_{10}$(sn-1) and (e) βBCMal-C$_{12}$C$_{10}$(sn-2). (TIF)

Figure S4   Schematic representations of the phase structures characterized for tetradecyl β-maltoside (βC$_{14}$G$_2$). (Redrawn from *Ericsson et al.*[18]) (TIF)

Figure S5   Correlation functions for each C–H vector along lipid alkyl chains are shown. The legend shows the carbon atoms following the numbering in Figure 1. (TIF)

Figure S6   Second rank reorientational autocorrelation functions $C_2(t)$ for the sugars at the headgroup region for all the four glycosides, namely, βMal-C$_{12}$, βCel-C$_{12}$, βIsoMal-C$_{12}$, and βBCMal-C$_{12}$C$_{10}$ for (a) non-reducing sugar (*ring1*), (b) reducing sugar (*ring2*) and (c) both the sugars together (*ring12*). (TIF)

Table S1   Dihedral angles (in degrees) for glycosides at the glycosidic bond between the two sugar units. (DOC)

Table S2   Phase transition temperatures for glycosides in an anhydrous condition from literatures. The lamellar distance of bilayers, *d* (in Å). (DOC)

Video S1   A movie showing the last 160 ns production, focusing only on one lipid (VDW model) in the third leaflet which tries to burrow one of its chains into the hydrophilic region in the simulation box. The head group region is represented by the wire frame model. (AVI)

Video S2   A movie of the top view of the lipid headgroup region for 160 ns. For clarity the hydrophobic part has been removed to show the hydrophobic cavity within the headgroup. (AVI)

Acknowledgments

Author Contributions

Conceived and designed the experiments: RAB RH VMA. Performed the experiments: VMA. Analyzed the data: RAB RH VMA. Contributed reagents/materials/analysis tools: RAB RH. Wrote the paper: RAB RH VMA.

References

1. Garelli-Calvet R, Brisset F, Rico I, Lattes A (1993) Bis-gluconamides and bis-lactobionamides novel α,ω-type (bolaform) surfactants with two sugar head groups. Synth Commun 23: 35–44.
2. Kiwada H, Niimura H, Fujisaki Y, Yamada S, Kato Y (1985) Application of synthetic alkyl glycoside vesicles as drug carriers. I. Preparation and physical properties. Chem Pharm Bull (Tokyo) 33: 753–759.
3. Brundish D, Shaw N, Baddiley J (1966) Bacterial glycolipids. Glycosyl diglycerides in gram-positive bacteria. Biochem J 99: 546–549.
4. Dörmann P, Hölzl G (2010) The role of glycolipids in photosynthesis. Lipids in Photosynthesis: Essential and regulatory functions. Dordrecht, Netherlands: Springer. pp. 265–282.
5. Hashim R, Sugimura A, Minamikawa H, Heidelberg T (2011) Nature-like synthetic alkyl branched-chain glycolipids: a review on chemical structure and self-assembly properties. Liq Cryst 39: 1–17.
6. Goodby JW, Gortz V, Cowling SJ, Mackenzie G, Martin P, et al. (2007) Thermotropic liquid crystalline glycolipids. Chem Soc Rev 36: 1971–2032.
7. Vill V, Hashim R (2002) Carbohydrate liquid crystals: structure–property relationship of thermotropic and lyotropic glycolipids. Curr Opin Colloid Interface Sci 7: 395–409.
8. Jayaraman N, Singh MK, Rao DS, Prasad S (2007) Studies of the mesomorphic behavior of bivalent carbohydrate amphiphiles. J Mater Chem 17: 2228–2232.
9. Ahmad N, Ramsch R, Esquena J, Solans C, Tajuddin HA, et al. (2012) Physicochemical characterization of natural-like branched-chain glycosides toward formation of hexosomes and vesicles. Langmuir 28: 2395–2403.
10. Sakya P, Seddon J, Vill V (1997) Thermotropic and lyotropic phase behaviour of monoalkyl glycosides. Liq Cryst 23: 409–424.
11. Singer SJ, Nicolson GL (1972) The fluid mosaic model of the structure of cell membranes. Science 175: 720–731.
12. Lewis RNAH, McElhaney RN (1992) The mesomorphic phase behavior of lipid bilayers. In: Yeagle P, editor. The structure of biological membranes. Boca Raton, Florida: CRC Press. pp. 73–155.
13. Cullis Pt, De Kruijff B (1979) Lipid polymorphism and the functional roles of lipids in biological membranes. BBA-Rev Biomembranes 559: 399–420.
14. Kulkarni CV (2012) Lipid crystallization: from self-assembly to hierarchical and biological ordering. Nanoscale 4: 5779–5791.
15. Abe Y, Harata K, Fujiwara M, Ohbu K (1998) Bilayer structure of glycolipid crystals. Thermal stability of the crystal and state of the alkyl chain. J Chem Soc, Perkin Trans 2: 177–186.
16. Kasson PM, Pande VS (2004) Molecular dynamics simulation of lipid reorientation at bilayer edges. Biophys J 86: 3744–3749.
17. Shinoda W, Mikami M, Baba T, Hato M (2003) Molecular dynamics study on the effect of chain branching on the physical properties of lipid bilayers: structural stability. J Phys Chem B 107: 14030–14035.
18. Ericsson CA, Ericsson LC, Kocherbitov V, Soderman O, Ulvenlund S (2005) Thermotropic phase behaviour of long-chain alkylmaltosides. Phys Chem Chem Phys 7: 2970–2977.
19. Auvray X, Petipas C, Dupuy C, Louvet S, Anthore R, et al. (2001) Small-angle x-ray diffraction study of the thermotropic and lyotropic phases of five alkyl cyclic and acyclic disaccharides: Influence of the linkage between the hydrophilic and hydrophobic moieties. Eur Phys J E 4: 489–504.
20. Doxastakis M, Sakai VG, Ohtake S, Maranas J, De Pablo J (2007) A molecular view of melting in anhydrous phospholipidic membranes. Biophys J 92: 147–161.
21. Klaus G (2005) The dynamics of membrane lipids. In: Yeagle PL, editor. The Structure of biological membranes. 2nd ed. Boca Raton, Florida: CRC Press. pp. 147–171.
22. Manickam Achari V, Nguan HS, Heidelberg T, Bryce RA, Hashim R (2012) Molecular dynamics study of anhydrous lamellar structures of synthetic glycolipids: Effects of chain branching and disaccharide headgroup. J Phys Chem B 116: 11626–11634.
23. Ham JT, Williams DG (1970) The crystal and molecular structure of methyl β-cellobioside-methanol. Acta Crystallogr B 26: 1373–1383.
24. McNaught AD (1996) International Union of Pure and Applied Chemistry and International Union of Biochemistry and Molecular Biology - Joint Commission on Biochemical Nomenclature - Nomenclature of carbohydrates - Recommendations 1996. Pure Appl Chem 68: 1919–2008.
25. Ott KH, Meyer B (1996) Molecular dynamics simulations of maltose in water. Carbohydr Res 281: 11–34.
26. Jeffrey GA, Huang DB (1991) Hydrogen bonding in the crystal structure of alpha,beta-panose. Carbohydr Res 222: 47–55.

27. HyperChem(TM) H, Inc., 1115 NW 4th Street, Gainesville, Florida 32601 USA HyperChem(TM), Hypercube, Inc., 1115 NW 4th Street, Gainesville, Florida 32601 USA.

28. Gentilcore A (2009) A multiscale computational investigation of forces between lipid bilayers. Baltimore, Maryland: Johns Hopkins University

29. Abe Y, Fujiwara M, Ohbu K, Harata K (2000) Crystal structures of glycolipids with odd and even numbered alkyl chains. J Chem Soc, Perkin Trans 2: 341–351.

30. Abeygunaratne S, Chien LC, Vill V (2007) Tilted supramolecular structures of amphiphilic glycolipids in straight-core smectic C liquid crystals. Liq Cryst 34: 441–445.

31. Hashim R, Hashim HHA, Rodzi NZM, Hussen RSD, Heidelberg T (2006) Branched chain glycosides: Enhanced diversity for phase behavior of easily accessible synthetic glycolipids. Thin Solid Films 509: 27–35.

32. Case DA, Darden TA, Cheatham I, Simmerling CL, Wang J, et al. (2006) AMBER 9 San Francisco: University of California.

33. Kirschner KN, Yongye AB, Tschampel SM, Gonzalez-Outeirino J, Daniels CR, et al. (2008) GLYCAM06: a generalizable biomolecular force field. Carbohydrates. J Comput Chem 29: 622–655.

34. Andrea TA, Swope WC, Andersen HC (1983) The role of long ranged forces in determining the structure and properties of liquid water. J Chem Phys 79: 4576–4584.

35. Ryckaert J-P, Ciccotti G, Berendsen HJC (1977) Numerical integration of the cartesian equations of motion of a system with constraints: molecular dynamics of n-alkanes. J Comput Phys 23: 327–341.

36. Miyamoto S, Kollman PA (1992) Settle - an analytical version of the Shake and Rattle Algorithm for rigid water models. J Comput Chem 13: 952–962.

37. Essmann U, Perera L, Berkowitz ML, Darden T, Lee H, et al. (1995) A smooth particle mesh Ewald method. J Chem Phys 103: 8577–8593.

38. Darden T, York D, Pedersen L (1993) Particle mesh Ewald: An N· log (N) method for Ewald sums in large systems. J Chem Phys 98: 10089.

39. Anézo C, de Vries AH, Höltje H-D, Tieleman DP, Marrink S-J (2003) Methodological issues in lipid bilayer simulations. J Phys Chem B 107: 9424–9433.

40. Nagle JF, Tristram-Nagle S (2001) Structure and interaction of lipid bilayers: Role of fluctuation; Gutberlet T, Katsaras J, editors: Springer.

41. Högberg C-J, Maliniak A, Lyubartsev AP (2007) Dynamical and structural properties of charged and uncharged lidocaine in a lipid bilayer. Biophys Chem 125: 416–424.

42. Róg T, Murzyn K, Gurbiel R, Takaoka Y, Kusumi A, et al. (2004) Effects of phospholipid unsaturation on the bilayer nonpolar region a molecular simulation study. J Lipid Res 45: 326–336.

43. Damodaran KV, Merz KM, Gaber BP (1992) Structure and dynamics of the dilauroylphosphatidylethanolamine lipid bilayer. Biochemistry 31: 7656–7664.

44. Mizushima S-I, Morino Y, Nozri S (1936) Raman effect and free rotation. Nature 137: 945–945.

45. Jeffrey GA, Wingert LM (1992) Carbohydrate liquid crystals. Liq Cryst 12: 179–202.

46. Niemelä P, Hyvönen MT, Vattulainen I (2004) Structure and dynamics of sphingomyelin bilayer: insight gained through systematic comparison to phosphatidylcholine. Biophys J 87: 2976–2989.

47. Hamid HA, Hashim R, Seddon JM, Brooks NJ (2014) Lyotropic phase behaviour and structural parameters of monosaccharide and disaccharide Guerbet branched-chain β-D-glycosides. Adv Mat Res 895: 111–115.

48. Lipowsky R (2013) Spontaneous tubulation of membranes and vesicles reveals membrane tension generated by spontaneous curvature. Faraday Discuss 161: 305–331.

49. Domanov YA, Kinnunen PK (2006) Antimicrobial peptides temporins B and L induce formation of tubular lipid protrusions from supported phospholipid bilayers. Biophys J 91: 4427–4439.

50. Niemelä PS, Hyvönen MT, Vattulainen I (2006) Influence of chain length and unsaturation on sphingomyelin bilayers. Biophys J 90: 851–863.

51. Humphrey W, Dalke A, Schulten K (1996) VMD: Visual molecular dynamics. J Mol Graphics 14: 33–38.

52. Kocherbitov V, Söderman O (2004) Glassy crystalline state and water sorption of alkyl maltosides. Langmuir 20: 3056–3061.

53. Small DM (1984) Lateral chain packing in lipids and membranes. J Lipid Res 25: 1490–1500.

54. Tardieu A, Luzzati V, Reman F (1973) Structure and polymorphism of the hydrocarbon chains of lipids: a study of lecithin-water phases. J Mol Biol 75: 711–733.

55. Carrier D, Giziewicz J, Moir D, Smith IC, Jarrell HC (1989) Dynamics and orientation of glycolipid headgroups by ^{2}H-NMR: gentiobiose. BBA-Biomembrane 983: 100–108.

56. Moore PB, Lopez CF, Klein ML (2001) Dynamical properties of a hydrated lipid bilayer from a multinanosecond molecular dynamics simulation. Biophys J 81: 2484–2494.

57. Essmann U, Berkowitz ML (1999) Dynamical properties of phospholipid bilayers from computer simulation. Biophys J 76: 2081–2089.

58. Róg T, Vattulainen I, Bunker A, Karttunen M (2007) Glycolipid membranes through atomistic simulations: effect of glucose and galactose head groups on lipid bilayer properties. J Phys Chem B 111: 10146–10154.

59. Lemieux R (1989) Rhône-Poulenc Lecture. The origin of the specificity in the recognition of oligosaccharides by proteins. Chem Soc Rev 18: 347–374.

60. Jimenez-Barbero J, Junquera E, Martin-Pastor M, Sharma S, Vicent C, et al. (1995) Molecular recognition of carbohydrates using a synthetic receptor. A model system to understand the stereoselectivity of a carbohydrate-carbohydrate interaction in water. J Am Chem Soc 117: 11198–11204.

61. Balasubramanian D, Raman B, Sundari CS (1993) Polysaccharides as amphiphiles. J Am Chem Soc 115: 74–77.

62. Misran O, Timimi BA, Heidelberg T, Sugimura A, Hashim R (2013) Deuterium NMR investigation of the lyotropic phases of alkyl β-glycoside/D$_2$O systems. J Phys Chem B 117: 7335–7344.

63. Huang C-h, Li S (1999) Calorimetric and molecular mechanics studies of the thermotropic phase behavior of membrane phospholipids. BBA-Rev Biomembranes 1422: 273–307.

64. Naidoo KJ, Kuttel M (2001) Water structure about the dimer and hexamer repeat units of amylose from molecular dynamics computer simulations. J Comput Chem 22: 445–456.

65. Mitchell FL, Miles SM, Neres J, Bichenkova EV, Bryce RA (2010) Tryptophan as a Molecular Shovel in the Glycosyl Transfer Activity of Trypanosoma cruzi Trans-sialidase. Biophys J 98: L38–L40.

66. Vandenbussche S, Díaz D, Fernández-Alonso MC, Pan W, Vincent SP, et al. (2008) Aromatic–carbohydrate interactions: an NMR and computational study of model systems. Chem-Eur J 14: 7570–7578.

67. Chen C, Berns D, Berns A (1981) Thermodynamics of carbohydrate-lipid interactions. Biophys J 36: 359–367.

68. Gurtovenko AA, Vattulainen I (2007) Molecular mechanism for lipid flip-flops. J Phys Chem B 111: 13554–13559.

69. Yamashita I, Kawabata Y, Kato T, Hato M, Minamikawa H (2004) Small angle X-ray scattering from lamellar phase for β-3, 7-dimethyloctylglucoside/water system: comparison with β- n-alkylglucosides. Colloid Surface A 250: 485–490.